# Postfault Operation of Three-Level Inverter Driven Six-Phase PMSM With Enhanced Torque–Speed Region

Partha Pratim Das, *Member, IEEE*, Subhransu Satpathy, *Member, IEEE*, and Subhashish Bhattacharya, *Fellow, IEEE*

***Abstract*—This article presents an open-switch postfault operational technique with enhanced torque–speed region for three-level (3L) active neutral point clamped (ANPC) inverter-driven symmetrical six-phase (SSP) permanent magnet synchronous machines (PMSMs). Maximum torque (MT), minimum loss (ML), and single three-phase (STP) operations are commonly used for the postfault operations of six-phase drives. The maximum possible torque and speed in these operations are generally limited by voltage, current ratings, and the neutral point configuration of the motor. To enhance the postfault torque and speed operating region, the torque and speed limits in different postfault operational techniques are determined based on the voltage, current constraints, and neutral point configuration of the SSP-PMSM. In this work, a unified postfault operation is proposed that increases the postfault operational limits by combining MT, ML, and STP operations and modifying the neutral point configuration of the SSP-PMSM. In addition, a technique is also presented that modifies the pulsewidth modulation technique to enable full torque operation below 0.5 p.u. speed. The proposed postfault operational technique enables full-speed (1 p.u.) operation by operating in STP mode and full torque operation (1 p.u.) below 0.5 p.u. speed. The postfault operational technique is experimentally validated using a Gallium Nitride (GaN) device-based 3L-ANPC inverter-driven SSP-PMSM.**

***Index Terms*—Maximum torque (MT), minimum loss (ML), multilevel inverter, multiphase drives, open-circuit fault (OCF), postfault operation, single-three phase (STP).**

## NOMENCLATURE

*General*

| | |
|---|---|
| $\vec{I_s}$ | Six-phase current vector. |
| $\vec{V_s}$ | Six-phase voltage vector. |
| $I_m$ | Rated current peak. |
| $\theta_r$ | Rotor position with respect to the $R$ phase magnetic axis. |
| $\omega_r$ | Rotor electrical speed in rad/sec. |
| $\omega_t$ | Critical speed in rad/sec (electrical speed). |
| $P_l$ | Number of poles. |
| $K_t$ | Torque constant. |
| $T$ | Motor electromagnetic torque. |
| $i_p$ | $p$ phase current. $p = r, y, b, u, v, w$. |
| $a_p$ | Cosine component of the $p$ phase current. |
| $b_p$ | Sine component of the $p$ phase current. |
| $k_p$ | Fraction of rated current being supplied. |
| $V_{\text{ll,rated,peak}}$ | Rated line to line voltage peak of the motor. |
| $r_s$ | Stator resistance. |
| $L_{\text{ls}}$ | Leakage inductance. |
| $L_d, L_q$ | $dq$-axis inductances. |
| $V_{\text{pm}}$ | Pole voltage of $p$ phase. |
| $\lambda_m$ | Permanent magnet flux linkage. |

*Subscripts and superscripts*

| | |
|---|---|
| $\square_{d1}, \square_{q1}, \square_{01}$ | $d$–$q$–0 axis variables of $RYB$ phases. |
| $\square_{d2}, \square_{q2}, \square_{02}$ | $d$–$q$–0 axis variables of $UVW$ phases. |
| $\square_d, \square_q, \square_{z1,z2}$ | $d$–$q$–0 axis variables of six-phases. |
| $\square_x, \square_y$ | $x$–$y$ axis variables of six-phases. |
| $\square_{\text{MT}}$ | Variable at maximum torque (MT) operation. |
| $\square_{\text{ML}}$ | Variable at minimum loss (ML) operation. |
| $\square_{\text{STP}}$ | Variable at single three-phase (STP) operation. |
| $\square_{\text{max}}$ | Maximum possible value. |
| $\square_{1N}$ | Variable in the $1N$ configuration. |
| $\square_{2N}$ | Variable in the $2N$ configuration. |
| $\square_{\text{rated}}$ | Rated voltage. |
| $\square_{\text{peak}}$ | Peak voltage. |
| $\square_{\text{base}}$ | Base speed of the motor. |
| $\square_b$ | Base speed in any particular operation. |
| $\square^*$ | Reference value. |
| $\square_{\omega t}$ | Variable at $\omega_t$ speed. |
| $\square^+$ | Positive sequence. |
| $\square^-$ | Negative sequence. |

Received 8 July 2024; revised 3 October 2024; accepted 9 November 2024. Date of publication 14 November 2024; date of current version 28 January 2025. This work supported by the U.S. Department of Energy, Office of Energy Efficiency and Renewable Energy, Vehicle Technology Office under Grant DE-EE0008705. Recommended for publication by Associate Editor Ebrahim Babaei. *(Corresponding author: Partha Pratim Das.)*

Partha Pratim Das and Subhashish Bhattacharya are with the ECE department, North Carolina State University, Raleigh, NC 27695 USA (e-mail: ppdas@ncsu.edu; sbhatta4@ncsu.edu).

Subhransu Satpathy is with the Texas Instruments Inc., Dallas, TX 75243 USA (e-mail: ssatpat2@ncsu.edu).

Color versions of one or more figures in this article are available at https://doi.org/10.1109/TPEL.2024.3498454.

Digital Object Identifier 10.1109/TPEL.2024.3498454

## I. INTRODUCTION

MULTIPHASE machines are popular alternatives to the three-phase machines due to their high fault-tolerant capability and reduced power rating of per-phase power electronics [1], [2], [3], [4]. Symmetrical six-phase (SSP)-permanent magnet synchronous machine (PMSM) (SSP-PMSM) is one of

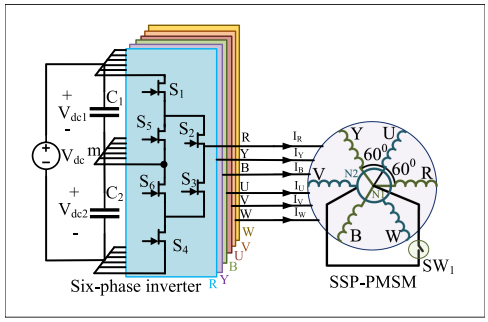


Fig. 1. Circuit diagram of a six-phase 3L-ANPC inverter with an SSP-PMSM. The $1N$ and $2N$ configurations of SSP-PMSM can be interchanged by turning ON and OFF $SW_1$, respectively.

the most popular multiphase machines for its easy construction, high fault-tolerant capability, and low-common-mode voltage [3], [5], [6]. In SSP-PMSM, two sets of three-phase windings ($RYB$ and $UVW$) are spatially shifted by 60°. The winding diagram of an SSP-PMSM is shown in Fig. 1. SSP-PMSMs have two types of winding configurations depending on the neutral point connections of the $RYB$ ($N1$) and the $UVW$ ($N2$) phases. The neutral point configurations are designated as $1N$ and $2N$ if $N1$ and $N2$ are connected and separate, respectively [3]. The $N1$ and $N2$ are connected to a switch ($SW_1$) in Fig. 1. By turning $SW_1$ ON and OFF, the winding configuration can be interchanged between $1N$ and $2N$ configurations. In this work, a Gallium Nitride (GaN) device-based three-level (3L)-active neutral point clamped (ANPC) inverter is considered for driving an SSP-PMSM for lower line current total harmonic distortion (THD), lower bearing current due to a lower effective $dv/dt$ compared to two-level (2L) inverters, and higher efficiency at high-switching frequency [7], [8], [9].

The postfault operation enables operations at a reduced power level in the case of common failure in any system. Incorporating postfault operation to increase reliability has become a crucial part of safety-critical electric drives like drives of electric transport systems [10], [11], [12], [13]. The postfault operation reduces the downtime of electric drives and can improve the safety and reliability of electric drives [14], [15]. The implementation of the postfault operation commonly has two parts. They are (a) fault detection and localization [16], [17], [18] and (b) software and hardware reconfiguration for postfault operation [19], [20], [21], [22], [23]. Dedicated algorithms are commonly used for fast detection and localization of faults [16], [17], [18]. After fault detection and localization, software and hardware are generally reconfigured for postfault operation [19], [20], [21], [22], [23]. This article focuses on the postfault operational technique to enhance the operating region of 3L-ANPC inverter-driven SSP-PMSMs. This article considers the postfault operation for a single open-switch failure. The first detection, localization, and implementation of postfault operation reduce the possibility of cascading failures [23].

The main aim of this article is to enable maximum postfault torque-speed operational region. The maximum possible postfault torque and speed limits are generally decided by voltage, current ratings, and the neutral point configuration of the motor.

TABLE I
MAXIMUM POSSIBLE TORQUE LIMIT WITH FIVE HEALTHY PHASES FOR ASP AND SSP-PMSM [3]

| Types of six-phase PMSM | $1N$ configuration | $2N$ configuration |
|---|---|---|
| ASP-PMSM | 0.694p.u. | 0.577p.u. |
| SSP-PMSM | 0.771p.u. | 0.5p.u. |

In this work, software and hardware modifications are used to increase postfault torque–speed operational limits of 3L-ANPC inverter-driven SSP-PMSM. In this work, the phase currents are limited to 1 p.u. in postfault operation to avoid overheating in the steady-state operation of the inverter and motor [3], [19], [21], [22], [23].

In the case of any failures of six-phase drives, the faulty phase is commonly disconnected, and the motor is operated with the remaining healthy phases [3], [19], [21]. In postfault operation, the current references of the healthy phases are commonly modified to generate uninterrupted torque by keeping the air gap flux sinusoidal [3], [19]. Three types of postfault operational techniques are commonly used in the literature. They are

1) single three-phase (STP) [20];
2) minimum loss (ML) [3], [24];
3) maximum torque (MT) [3], [24].

In case of a fault in any one phase, the corresponding three-phase set is turned-OFF, and the motor is operated with the healthy three-phase set in the STP operation. For example, if a fault is detected in the $R$ phase, the $RYB$ phases are turned-OFF, and the motor is controlled using $UVW$ phases. Consequently, in the STP operation, the torque gets limited to 0.5 p.u. without violating the current rating of the motor [20]. In STP operation, the healthy two phases from the faulty three-phase set remain unused. In MT and ML operations, all five healthy phases are used to enhance torque output in postfault operations. In the ML operation, the copper loss is minimized to generate a given torque [3], [20]. However, ML operation generates unequal loading for all the healthy phases. The maximum possible torque generation capability in the ML operation is also low. For SSP-PMSM, the maximum possible torque generation capabilities in the ML operation for one phase fault are 0.688 p.u. and 0.5 p.u. in $1N$ and $2N$ configurations, respectively [3]. The maximum possible torque generation capability is enhanced in MT operation. In the MT operation, torque generation is increased by maximization of the current of all healthy phases [3], [20], [24]. The MT operation enables higher torque generation at the expense of higher copper loss than the ML operation [3]. The detailed MT and ML operational techniques and their operation limits are provided in Section II. The maximum possible torque limits using healthy five phases are given in Table I [3].

The combinations of STP, ML, and MT operations in different operating zones can improve postfault torque–speed operational limits and reduce copper loss simultaneously. In [24], ML and MT operations are combined to increase the operating region of 2L inverter-driven asymmetrical six-phase (ASP)-PMSM. In ASP-PMSM, two three-phase windings are spatially shifted by 30°. The maximum possible torque limit using MT operation is provided in Table I [3]. The maximum possible torque output is

limited to 0.694 p.u. for a single-phase fault using the method of [24]. In [19], one full range ML technique is proposed for 2L-inverter-driven ASP-PMSM in the $2N$ configuration. However, the maximum possible torque is limited to 0.577 p.u. for one phase fault. Hence, it is not considered further in this work. In [20], STP, MT, and ML operations are combined for 2L-inverter-driven ASP-PMSM in the $2N$ configuration. However, in [20], the maximum possible torque is limited to 0.577 p.u. In the case of SSP-PMSM, the maximum possible torque limit in the $2N$ configuration with five healthy phases is 0.5 p.u., which is the same as the STP mode of operation [3]. In the abovementioned techniques, the neutral point configuration is kept fixed. The fixed neutral point configuration limits the maximum possible torque-speed region in the postfault operation [21].

In [21], switching between $1N$ and $2N$ configurations is proposed to enhance the torque–speed limit of 2L inverter-driven ASP-PMSM. In the $2N$ configuration, the postfault torque is limited to a lower value than in the $1N$ configuration, as shown in Table I. On the other hand, in the $1N$ configuration of the six-phase motors, the maximum speed gets limited due to low dc bus utilization and the maximum line-to-line voltage rating of the motor [21], [25]. In [21], the ASP-PMSM is operated in the $1N$ configuration to achieve a maximum possible torque of 0.694 p.u. in the low-speed operation. The ASP-PMSM is operated in the $2N$ configuration during high-speed operations to enhance the speed limit. However, the maximum possible torque in [21] is still limited to 0.694 p.u. A technique for torque enhancement below 0.5 p.u. speed is proposed in [22] for open-switch faults. In [22], the pole of the faulty phase is connected to the midpoint of the dc bus to enhance the postfault operational torque limit. The method of [22] achieves 1 p.u. torque below 0.5 p.u. speed for 2L inverter-driven ASP induction motors. Above 0.5 p.u. speed, the motor is operated with all healthy phases in the $1N$ configuration to enhance the torque limit. In [22], contactors are used to connect the faulty phase to the midpoint of the dc bus. However, the method of [22] does not consider $2N$ configuration or STP operation at high speed, which limits the maximum speed of the motor. Connecting the faulty phase pole to the midpoint of the dc bus to enhance torque limit is also used for 3L inverter-driven ASP-PMSMs in [23] and [26]. In [23] and [26], triodes for alternating current (TRIACs) are used to connect the faulty phase pole to the midpoint of the dc bus. However, in [23] and [26], the motor is only operated in the $2N$ configuration, which can limit the maximum possible torque to 0.577 p.u. above 0.5 p.u. speed. Moreover, the methods of [22], [23], [26] need extra hardware to connect the faulty phase pole to the midpoint of the dc bus. The extra hardware increases the cost of the system and reduces power density. In this article, an open-switch postfault control technique is presented that can deliver 1 p.u. torque below 0.5 p.u. speed without the need for any additional hardware for connecting the faulty phase pole to the mid-point of the dc bus. The method takes advantage of the extra available switches of the 3L-ANPC topology to generate 1 p.u torque below 0.5 p.u. speed. In addition, a unified postfault operational technique is proposed that combines $1N$ and $2N$ configurations with MT, ML, and STP modes of operation. The unified technique of 2L, MT, and ML operation with $1N$ and $2N$ configurations enables maximum possible torque-speed region. Fig. 2 compares the possible postfault torque–speed region with available methods of the literature.

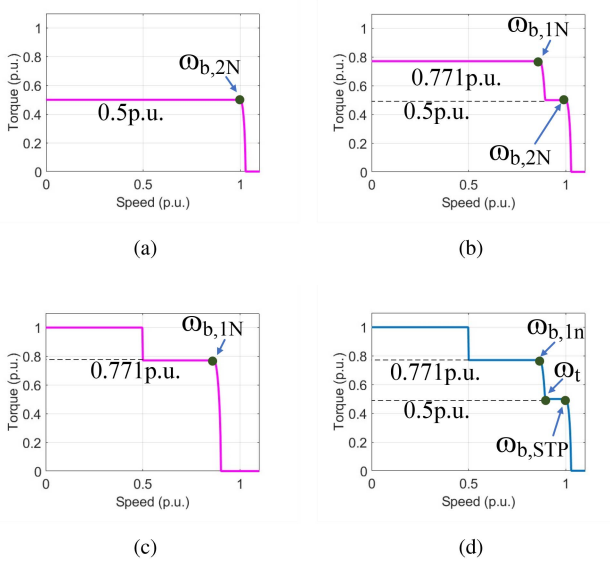


Fig. 2. Comparison of postfault torque–speed region with the available method of the literature for SSP-PMSM. (a) Torque–speed region of [19], [20]. (b) Torque–speed region of [21]. (c) Torque–speed region of [22]. This method needs additional hardware to connect the faulty phase to the midpoint of the dc bus. (d) Torque–speed region of this article. This method does not need additional hardware to connect the faulty phase to the midpoint of the dc bus.

The proposed technique enables 1 p.u. torque generation below 0.5 p.u. speed. Consequently, compared to the operation with healthy five phases, the torque output limit increases by 29.7%. Above 0.5 p.u. speed, the proposed technique maximizes the torque output limit to 0.771 p.u. by operating the SSP-PMSM in the $1N$ configuration. The proposed technique maximizes the speed output limit by operating the inverter in the STP mode above critical speed ($\omega_t$). The STP operation enables operation at 1 p.u. speed without field weakening (increased by 15.47% from 0.866 to 1 p.u.).

The proposed technique does not use additional hardware to connect the faulty phase pole to the mid-point of the dc bus. However, the proposed technique uses $SW_1$ to switch between $1N$ and $2N$ configurations. The $SW_1$ is commonly used to maximize torque output in the postfault operation of six-phase drives [21], [22].

Table II compares the available postfault operational techniques with the proposed technique of this article. The available techniques can generate 1 p.u. torque below 0.5 p.u. speed with additional hardware. However, the method proposed in this article does not need additional hardware to generate 1 p.u. torque below 0.5 p.u. speed. Moreover, the method proposed in this article enhances the speed torque region by switching between $1N$ and $2N$ configurations. The contributions of this article are summarized as follows.

1) Proposing a postfault operation technique that achieves 1 p.u. torque below 0.5 p.u. speed without the need for

TABLE II
COMPARISON OF POSTFAULT OPERATIONS OF SIX-PHASE MOTOR DRIVES

| Reference | Full torque operation (1 p.u. torque) below 0.5p.u. speed | Torque maximization above 0.5p.u. speed and below base speed | Speed maximization above base speed | Additional hardware requirement |
|---|---|---|---|---|
| [19], [20] | × | × | ✓ | No |
| [21] | × | ✓ | ✓ | No |
| [22] | ✓ | ✓ | × | Yes |
| [23] | ✓ | × | ✓ | Yes |
| **This article** | ✓ | ✓ | ✓ | **No** |

The bold text highlights the applicability of this article with that of the literature.

any additional hardware to connect the faulty phase pole to the midpoint of the dc bus.

2) Proposing a unified postfault operation that achieves maximum possible torque speed region. The $1N$ configuration of the motor maximizes the postfault torque limit. The $2N$ configuration or STP mode of operation maximizes the speed limit. In this work, a unified postfault operational technique is proposed that combines $1N$ and $2N$ configurations with MT, ML, and STP modes of operation. The proposed postfault operational technique enables 0.771 p.u. torque above 0.5 p.u. speed by operating the SSP-PMSM in the $1N$ configuration. The proposed postfault operational technique also increases the speed limit by operating the drive in the STP mode ($2N$) at high-speed operations.

The rest of this article is organized as follows. After the introduction, postfault operational torque limits using STP, MT, and ML techniques are discussed in Section II. The postfault operational speed limits and a method to enhance the postfault operating region are discussed in Section III. The pre- and postfault control technique of the SSP-PMSM is discussed in Section IV. The postfault operational technique is verified in a hardware prototype, and the results are presented in Section V. Finally, Section VI concludes this article.

## II. POSTFAULT OPERATION

STP, MT, and ML techniques are commonly used for postfault operations. In this section, torque limits using STP, MT, and ML techniques are determined. Vector space decomposition (VSD)-based modeling is commonly used for field-oriented control of SSP-PMSM. In the VSD-based modeling approach, six-phase variables are represented in three orthogonal two-dimensional subspaces named $d-q$, $x-y$, and $z_1-z_2$. Each variable in VSD-based modeling is given as

$$f_d = f_{d1} + f_{d2} \quad f_q = f_{q1} + f_{q2} \quad f_x = f_{q1} - f_{q2}$$
$$f_y = -f_{d1} + f_{d2} \quad f_{z1} = f_{01} \quad f_{z2} = f_{02}. \tag{1}$$

In (1), $f_{d1}$, $f_{q1}$, and $f_{z1}$ are the variables (voltage, current, flux, etc.) from the $RYB$ phases, and $f_{d2}$, $f_{q2}$, and $f_{z2}$ are the variables from the $UVW$ phases. The phase variables are converted to $d1$, $d2$, $q1$, $q2$, $z1$, and $z2$ axis variables using (2) and (3). $f_r$, $f_y$, $f_b$, $f_u$, $f_v$, and $f_w$ are the phase variables of $R$, $Y$, $B$, $U$, $V$, and $W$ phases, respectively

$$\begin{bmatrix} f_{q1} \\ f_{d1} \\ f_{01} \end{bmatrix} = \frac{1}{3} \begin{bmatrix} \cos(\theta_r) & \cos\left(\theta_r - \frac{2\pi}{3}\right) & \cos\left(\theta_r + \frac{2\pi}{3}\right) \\ -\sin(\theta_r) & -\sin\left(\theta_r - \frac{2\pi}{3}\right) & -\sin\left(\theta_r + \frac{2\pi}{3}\right) \\ 0.5 & 0.5 & 0.5 \end{bmatrix} \times \begin{bmatrix} f_r \\ f_y \\ f_b \end{bmatrix} \tag{2}$$

$$\begin{bmatrix} f_{q2} \\ f_{d2} \\ f_{02} \end{bmatrix} = \frac{1}{3} \begin{bmatrix} \cos(\theta_r - \frac{\pi}{3}) & \cos(\theta_r - \frac{3\pi}{3}) & \cos(\theta_r - \frac{5\pi}{3}) \\ -\sin(\theta_r - \frac{\pi}{3}) & -\sin(\theta_r - \frac{3\pi}{3}) & -\sin(\theta_r - \frac{5\pi}{3}) \\ 0.5 & 0.5 & 0.5 \end{bmatrix} \times \begin{bmatrix} f_u \\ f_v \\ f_w \end{bmatrix}. \tag{3}$$

The current vector of an SSP-PMSM is given as (4). In (4), $p = r, u, y, v, b$, and $w$ for $n$ =1 to 6. In healthy and balanced operating conditions without field weakening, $i_p$ is given as (5), where $\theta_r$ is the rotor position with respect to the $R$ phase magnetic axis. $I_m$ is the rated current peak, and $k_p$ is the fraction of the rated current being supplied. At rated healthy operating condition $k_p$ =1. From (4), $|\vec{I_s}| = k_p I_m$. $i_p$ is simplified and given as (6), where $a_p$ and $b_p$ are the current coefficients of the $p$ phase ($p = r, u, y, v, b$, and $w$). $a_p$ and $b_p$ are given as (7). $a_p$ and $b_p$ represent the current phase difference and the fraction of the rated current on any phase. To keep the current peak below the rated current, the $k_p$ should be limited to 1 ($k_p \leq 1$).

From (1) and (5) $\sqrt{I_q^2 + I_d^2} = k_p I_m = |\vec{I_s}|$. The electromagnetic torque of the motor is given as (8). $P_l$ is the number of poles. In the case of no field weakening ($I_d = 0$), the electromagnetic torque of the motor is given as (9). $K_t$ is the torque constant of the motor

$$\vec{I_s} = \frac{1}{3} \sum_{n=1}^{6} i_p e^{j(n-1)\frac{\pi}{3}} = k_p I_m e^{j\theta_r} \tag{4}$$

$$i_p = k_p I_m \cos\left(\theta_r - (n-1)\frac{\pi}{3}\right) \tag{5}$$

$$= I_m(a_p \cos\theta_r + b_p \sin\theta_r) \tag{6}$$

$$a_p = k_p \cos\left((n-1)\frac{\pi}{3}\right) \quad b_p = k_p \sin\left((n-1)\frac{\pi}{3}\right)$$

$$k_p = \sqrt{a_p^2 + b_p^2} \tag{7}$$

$$T = \frac{3P_l}{2}(\lambda_m I_q + (L_d - L_q) I_q I_d) \tag{8}$$

$$T = K_t I_q = K_t k_p I_m = K_t |\vec{I_s}| \quad [\text{when } I_d = 0]. \tag{9}$$

In healthy and rated operating conditions ($k_p$ =1), $a_p$ and $b_p$ can be derived as (10) [20], [27]

$$\sum_{n=1}^{6} a_p \cos\left((n-1)\frac{\pi}{3}\right) = 3 \quad \sum_{n=1}^{6} a_p \sin\left((n-1)\frac{\pi}{3}\right) = 0$$

$$\sum_{n=1}^{6} b_p \cos\left((n-1)\frac{\pi}{3}\right) = 0 \quad \sum_{n=1}^{6} b_p \sin\left((n-1)\frac{\pi}{3}\right) = 3. \tag{10}$$

Moreover, according to Kirchhoff's current law (KCL), the summation of all phase currents is zero in the $1N$ configuration under any operating conditions. In the $2N$ configuration, the summations of $RYB$ phase currents and $UVW$ phase currents are zero separately in any operating condition. In the $1N$ configuration, $a_p$ and $b_p$ are given as (11) [20], [27]

$$\sum_{p=r,y,b,u,v,w} a_p = 0 \qquad \sum_{p=r,y,b,u,v,w} b_p = 0. \tag{11}$$

In any operating condition, in the $2N$ configuration $\sum_{p=r,y,b} i_p = 0$, and $\sum_{p=u,v,w} i_p = 0$. Hence, $a_p$ and $b_p$ are given as (12) [20], [27]

$$\sum_{p=r,y,b} a_p = 0 \quad \sum_{p=r,y,b} b_p = 0 \quad \sum_{p=u,v,w} a_p = 0 \quad \sum_{p=u,v,w} b_p = 0. \tag{12}$$

One way to keep the torque of the machine unchanged in the postfault operation is by keeping the air gap flux or the current vector the same as in healthy conditions. To keep the current vector the same as the healthy condition, (10) and (11) or (12) should be followed in $1N$ and $2N$ configurations, respectively. In postfault operation, if the faulty phase is disconnected, the $a_p$ and $b_p$ of the faulty phase become zero. However, (10) must be followed to keep the current vector the same and generate 1 p.u. torque. Equations (11) and (12) must also be followed in $1N$ and $2N$ configurations, respectively, to abide by KCL. In the following section, the fault is considered in the $R$ phase. The same method can be used for calculating $a_p$ and $b_p$ values for other phase failures.

### A. STP Operation

In the case of the STP operation, the three-phase set, which consists of the faulty phase, is turned-OFF. In the case of a fault in the $R$ phase, $RYB$ phases are turned-OFF. A detailed analysis of the STP mode of operation is given in the Appendix. The calculated current vector in STP mode of operation is $|\vec{I}_s| = 0.5I_m$. The maximum possible torque capability in the STP operation ($T_{\text{stp,max}}$) is $\frac{T_{\text{stp,max}}}{T} = 0.5$ p.u. when the phase currents are limited to 1 p.u.

### B. MT Operation

In case of a failure, the faulty phase is turned-OFF, and the motor is operated with the remaining five healthy phases in MT operation. In MT operation, the peaks of all five healthy phase currents are controlled to the same value [3]. Hence, $a_p$ and $b_p$ are given as (13) for the $R$ phase failure

$$a_y^2 + b_y^2 = a_b^2 + b_b^2 = a_u^2 + b_u^2 = a_v^2 + b_v^2 = a_w^2 + b_w^2. \tag{13}$$

A detailed analysis of the MT mode of operation is given in the Appendix. The calculated current vector in the MT mode of operation is $|\vec{I}_s| = 0.771I_m$ in the $1N$ configuration. The maximum possible torque capability in the MT operation ($T_{\text{MT,max}}$) is $\frac{T_{\text{MT,max}}}{T} = 0.771$ p.u. when the phase currents are limited to 1 p.u.

Similarly, the torque limit is calculated in the $2N$ configuration. In the $2N$ configuration, the torque limit is 0.5 p.u. As the torque limit is less than the $1N$ configuration, the MT operation in the $2N$ configuration is not further considered in this work.

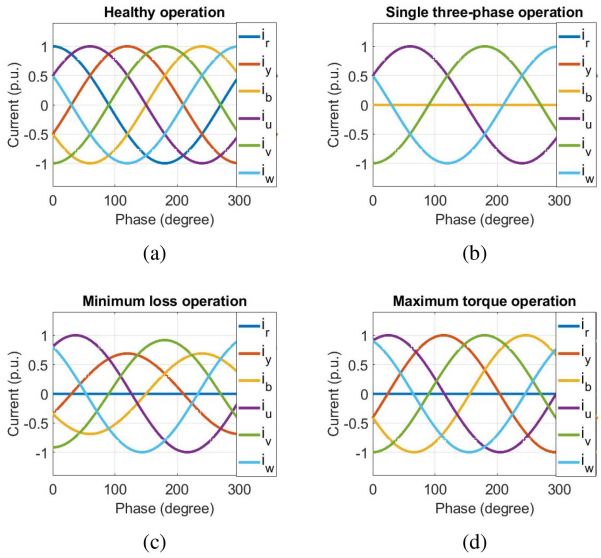


Fig. 3. Rated current in different operations for $R$ phase failure. (a) Healthy operation. The peak current of 1 p.u. generates 1 p.u. torque (b) STP operation. The peak current of 1 p.u. generates 0.5 p.u. torque. (c) ML operation. The $U$ phase has the maximum peak current. The peak current of 1 p.u. generates 0.688 p.u. torque. The current peaks for all phases are different. (d) MT operation. The peak current of 1 p.u. generates 0.771 p.u. torque. The current waveforms are plotted using the $a_p$ and $b_p$ variables of (32), (35), and (37).

### C. ML Operation

For ML operation, stator copper loss is minimized for a given torque. The copper loss coefficient ($J$) is defined by (14) for $R$ phase failure [3], [20]. $J$ is the square summations of the per unitized peaks. For ML operation, an optimization is used where $J$ is minimized to achieve a given torque

$$J = a_y^2 + b_y^2 + a_b^2 + b_b^2 + a_u^2 + b_u^2 + a_v^2 + b_v^2 + a_w^2 + b_w^2. \tag{14}$$

A detailed analysis of the ML mode of operation is given in the Appendix. The calculated current vector in the ML mode of operation is $|\vec{I}_s| = 0.688I_m$ in the $1N$ configuration. The maximum possible torque capability in the ML operation ($T_{\text{ML,max}}$) is $\frac{T_{\text{ML,max}}}{T} = 0.688$ p.u. when the phase currents are limited to 1 p.u.

Similarly, the torque limit is calculated in the $2N$ configuration. In the $2N$ configuration, the torque limit is 0.5 p.u. As the torque limit is less than the $1N$ configuration, the ML operation in the $2N$ configuration is not further considered in this work.

From the aforementioned discussion, the rated currents in different operations are plotted in Fig. 3. The torque limits in different operations are shown in Fig. 4(a).

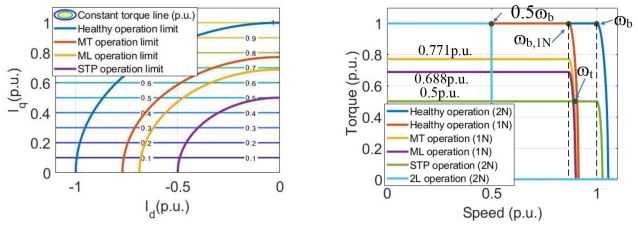


(a) (b)

Fig. 4. (a) Operational torque limits in healthy operation with all six phases and postfault operations. In the healthy operation, the torque limit is 1 p.u. In MT, ML, and STP operations, the torque limit is 0.771 p.u., 0.688 p.u., and 0.5 p.u., respectively. (b) Operational torque and speed limits in healthy operation and in postfault operations.

TABLE III
MOTOR PARAMETERS

| Parameter | $L_{md}$ ($\mu$H) | $L_{mq}$ ($\mu$H) | $L_{ls}$ ($\mu$H) | $r_s$ ($m\Omega$) | $\lambda_m$ ($mWb$) | Number of poles ($P_l$) | Rated current(rms) (A) |
|---|---|---|---|---|---|---|---|
| Value | 151 | 173 | 333 | 419 | 50 | 8 | 3.54 |

## III. POSTFAULT OPERATIONAL LIMIT ENHANCEMENT

The considered motor is a surface permanent magnet motor with a quasi-regular polygon rotor. The motor parameters are given in Table III. The saliency ratio of the motor ($\frac{L_q}{L_d}$) is close to 1 (1.069). Consequently, the MTPA line closely matches with the $I_d = 0$ line in the $dq$-axis current plane. Hence, below base speed, the $d$-axis current ($I_d$) is controlled to zero, or no field weakening is considered. Below base speed, the $I_d = 0$ and $I_q = |\vec{I_s}|$. Hence, in the STP operation, the torque and $q$-axis current should be limited to 0.5 p.u. In the MT operation, the torque and $q$-axis current should be limited to 0.771 p.u. In the ML operation, the torque and $q$-axis current should be limited to 0.688 p.u. The speed limits in different operations are discussed in the following section.

### A. Speed Limit

Line-to-line voltage constraints are commonly considered for determining speed limits [21], [25]. The peak of the line-to-line voltage should not cross the rated line-to-line voltage peak to avoid operating in the overmodulation zone and ensure the safety of the motor windings [21], [25]. In the $2N$ configuration, the neutral points are separate. For line-to-line voltage consideration in the $2N$ configuration, two three-phase sets ($RYB$ and $UVW$) are considered separately. The line-to-line voltage between any two phases of the same three-phase group ($RYB$ or $UVW$) is constant and given as $V_{ll,2N,\text{peak}} = \sqrt{3}|\vec{V_{s,2N}}|$. $\vec{V_{s,2N}}$ is the six-phase voltage vector in the $2N$ configuration. The six-phase voltage vector can be determined by replacing phase currents with phase voltages in (4). $V_{ll,2N,\text{peak}}$ is the peak of the line-to-line voltage in the $2N$ configuration. In the $1N$ configuration, due to the common neutral point, all six phases are considered under the same group. The maximum line-to-line voltage appears across the two 180° spatially shifted phases like $R$ and $V$, $U$ and $B$, and $Y$ and $W$. The minimum line-to-line voltage appears across the two 60° spatially shifted phases like $R$ and $U$. In the $1N$ configuration, the maximum line-to-line voltage peak is given as $V_{ll,1N,\text{peak}} = 2|\vec{V_{s,1N}}|$ as it appears across two 180° spatially shifted phases [21], [25]. $\vec{V_{s,1N}}$ is the six-phase voltage vector in the $1N$ configuration. $V_{ll,1N,\text{peak}}$ is the peak of the maximum line-to-line voltage in the $1N$ configuration. The motor line-to-line voltage peak should always be kept limited to the rated value for the safety of the motor. Moreover, the line-to-line voltage peak also determines the minimum dc bus voltage requirement for the drives [21], [25]. Hence, the voltage vectors in $1N$ and $2N$ configurations are given as (15). $V_{\text{ll,rated,peak}}$ is the rated peak of the line-to-line voltage

$$|\vec{V_{s,2N}}| \le \frac{V_{\text{ll,rated,peak}}}{\sqrt{3}} \quad |\vec{V_{s,1N}}| \le \frac{V_{\text{ll,rated,peak}}}{2}. \tag{15}$$

The commonly known voltage equation of the machine is given as (16). In (16), $r_s$ is the stator resistance. $L_{\text{ls}}$, $L_d$, and $L_q$ are the leakage, $d$, and $q$-axis inductances, respectively

$$\begin{aligned} V_d &= r_s I_d + L_d \frac{d}{dt} I_d - \omega_r L_q I_q \\ V_q &= r_s I_q + L_q \frac{d}{dt} I_q + \omega_r (\lambda_m + L_d I_d) \\ V_x &= r_s I_x + L_{ls} \frac{d}{dt} I_x \quad V_y = r_s I_y + L_{ls} \frac{d}{dt} I_y \\ V_{z1} &= r_s I_{z1} + L_{ls} \frac{d}{dt} I_{Z1} \quad V_{z2} = r_s I_{z2} + L_{ls} \frac{d}{dt} I_{Z2}. \end{aligned} \tag{16}$$

The base speed of any operation is the maximum speed without field weakening ($I_d = 0$) in that particular mode of operation. Below base speed, the voltage vector is given as (17). At the steady state, $I_d$ and $I_q$ are constants, and their derivative terms are zero. For voltage vector ($\vec{V_s}$) calculation, the effect of resistance drops ($r_s I_d$ and $r_s I_q$) are ignored. The $x$–$y$ and $z_1$–$z_2$ axis voltage values ($V_x, V_y, V_{z1}$, and $V_{z2}$) are also ignored due to low resistance and leakage inductance drops (resistance drop $< 1.67\%$ of back emf at base speed) (leakage inductance drop $< 0.53\%$ of back-EMF).

$$|\vec{V_s}| = V_d^2 + V_q^2 = (\omega_r L_q I_q)^2 + (\omega_r \lambda_m)^2. \tag{17}$$

The motor base speed in the $2N$ configuration is denoted as $\omega_b$. All the speed per unitizations in this article are done with respect to $\omega_b$. From (15) and (17), $\omega_b$ is given as (18)

$$\omega_b = \omega_{2N,\text{base}} = \frac{V_{\text{ll,rated,peak}}/\sqrt{3}}{\sqrt{(L_q I_q)^2 + (\lambda_m)^2}}. \tag{18}$$

From (15) and (17), the base speed in the $1N$ configuration is given as (19). Similarly, the base speeds of MT, ML, and STP operations are given as (20). In (20), the $I_q$ is replaced by the corresponding current limit calculated in Section II. In the base speed calculation, the assumption is $L_q I_q \ll \lambda_m$ and $\sqrt{(L_q(xI_q))^2 + (\lambda_m)^2} \approx \lambda_m$ where $x$ is a real positive number and $x \le 1$

$$\omega_{b,1N} = \frac{V_{\text{ll,rated,peak}}/2}{\sqrt{(L_q I_q)^2 + (\lambda_m)^2}} = \frac{\sqrt{3}}{2}\omega_b \tag{19}$$

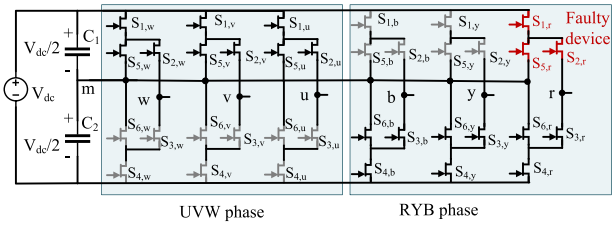


Fig. 5. Continuous operating (black) and unused (gray) devices for postfault 2L operation. For the example condition, an $OCF$ is considered in the $R$ phase's $S_1$, $S_2$, or $S_5$ device. The 2L voltage can be generated using $S_3$, $S_4$, and $S_6$ of $RYB$ phases and $S_1$, $S_2$, and $S_5$ devices of $UVW$ phases. This method generates equal loading for each half of the dc bus.

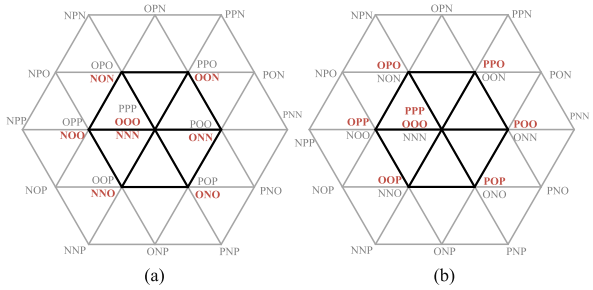


Fig. 6. Considered 2L-SVPWM below 0.5 p.u. speed for open-switch fault in $S_1, S_2$, or $S_5$ in the $R$ phase. (a) Used vectors for $RYB$ phases. (b) Used vectors for $UVW$ phases. Used vectors are marked in red.

$$\omega_{b,\mathrm{MT}} = \frac{V_{\mathrm{ll,rated,peak}}/2}{\sqrt{(L_q(0.771I_q))^2 + (\lambda_m)^2}} \approx \frac{\sqrt{3}}{2}\omega_b [\text{error} \leq 0.08\%]$$
$$\omega_{b,\mathrm{ML}} = \frac{V_{\mathrm{ll,rated,peak}}/2}{\sqrt{(L_q(0.688I_q))^2 + (\lambda_m)^2}} \approx \frac{\sqrt{3}}{2}\omega_b [\text{error} \leq 0.11\%]$$
$$\omega_{b,\mathrm{STP}} = \frac{V_{\mathrm{ll,rated,peak}}/\sqrt{3}}{\sqrt{(L_q(0.5I_q))^2 + (\lambda_m)^2}} \approx \omega_b \quad [\text{error} \leq 0.16\%]. \tag{20}$$

Above the base speed, a negative $d$-axis current is used for field weakening. During field weakening, the $d$-axis and maximum $q$-axis reference currents ($I_d^*$, $I_{q,\max}^*$) and speed are given as (21). $I_{q,\max}^*$ is the maximum $q$-axis reference current during field weakening operation. $\omega_{\mathrm{base}}$ is the base speed in any particular operation where field weakening is being considered. $\omega_r$ is the speed of the motor. $|\vec{I_{s,\mathrm{op}}}|$ the maximum current vector in any operation. For example, in STP operation $|\vec{I_{s,\mathrm{op}}}| = 0.5I_m$ and $|\vec{I_{s,\mathrm{op}}}| = 0.771I_m$ in the MT operation

$$I_d^* = \frac{(\frac{\omega_{\mathrm{base}}}{\omega_r} - 1)\lambda_m}{L_d}$$
$$I_{q,\max}^* = \sqrt{|\vec{I_{s,\mathrm{op}}}|^2 - I_d^{*2}}. \tag{21}$$

In the field weakening operation, the torque is given as (8). Using (8) and (19), the operational limits in different operations are plotted in Fig. 4(b).

The maximum possible torque limit is 0.771 p.u. for a single device fault in the MT operation. The torque limit can be further enhanced using the extra switching devices available in the 3L-ANPC topology. A method for further enhancement of the torque–speed region in the postfault operation is discussed in the following subsection.

### B. 2L Operation

In 2L operation, healthy switches of the faulty phase are used to generate 1 p.u. torque (increase by 29.7% from MT operation). In 3L inverters, pole voltage $V_{\mathrm{pm}}$ $(p = r, y, b, u, v, w)$ generates 3Ls of voltages $V_{\mathrm{dc}/2}, 0, -V_{\mathrm{dc}/2}$ designated as $P$, $O$, and $N$, respectively. Let us consider a case where a fault has happened in any one of $S_1$, $S_2$, or $S_5$ devices of the $R$ phase, as shown in Fig. 5. It is assumed that the devices have an open-switch fault and that no current can flow through the device. (In the case of devices with an antiparallel diode, diodes are in reverse bias, and no current can flow through them.) An open-circuit fault (OCF) in $S_1$ or $S_2$ causes the loss of the $P$ level in the $R$ phase. The OCF in $S_5$ causes the loss of $O$ level during the positive half cycle of the fundamental voltage. The remaining switches can be used to generate two voltage levels that vary between $N$ and $O$. For $N$ or $O$ voltage level generations, $S_3$ and $S_4$ or $S_3$ and $S_6$ should be turned-ON, respectively. As the voltage varies between 2Ls, $N$ and $O$, this operation is designated as the 2L operation.

A dual three-phase space vector pulse width modulation (SVPWM) technique is used in this article, where two 3L-three-phase SVPWM blocks are implemented to generate the six-phase voltages [23], [28]. The 3L-three-phase space vector diagrams are shown in Fig. 6. Fig. 6(a) and (b) are responsible for generating pulsewidth modulation (PWM) signals for the $RYB$ and $UVW$ phases, respectively. In the case of $S_1$, $S_2$, or $S_5$ device failure in the $R$ phase, any three-phase voltage vector generation that is inside the black color marked hexagon of Fig. 6(a) is possible. For the voltage generation, the red-marked switching states of Fig. 6(a) are used. The utilized switches are highlighted in black color in Fig. 5. The unused devices are marked in gray and red. Consequently, $S_3$, $S_4$, and $S_6$ devices of $RYB$ phases are used. However, operating only with the $S_3$, $S_4$, and $S_6$ devices discharges only the $C_2$ capacitor of the dc bus, resulting in a voltage unbalance between $C_1$ and $C_2$ capacitors. To eliminate the unbalance between $C_1$ and $C_2$, the $UVW$ phases are operated with $S_1, S_2$, or $S_5$ devices to generate 2L voltages. The maximum possible length of the voltage vector with continuous PWM is exactly half of the maximum possible length of the voltage vector of the large hexagon (see Fig. 6) with all healthy switches. To limit the voltage vectors inside the small marked hexagon, the 2L operation is limited to 0.5 p.u. speed. The operating limit for 2L operation is shown in Fig. 4(b). In the abovementioned 2L operation, the average common mode voltage between $N1$ and $m$ is $-\frac{V_{\mathrm{dc}}}{4}$, and $N2$ and m is $\frac{V_{\mathrm{dc}}}{4}$. Consequently, the average voltage between $N1$ and $N2$ is $\frac{V_{dc}}{2}$. The average dc voltage can generate a very high circulating current, depending on the stator resistance, between the $RYB$ and $UVW$ phases in the $1N$ configuration. Hence, for the 2L operation, the motor should only be operated in the $2N$

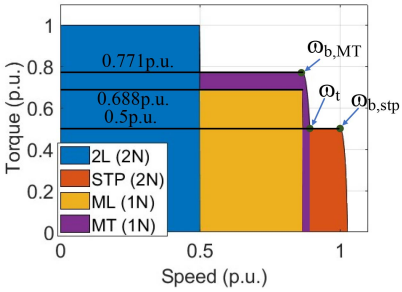


Fig. 7. Proposed postfault operational zones. (i) $\omega_r \leq 0.5$ p.u.: 2L operation to achieve 1 p.u. torque. (ii) 0.5 p.u. $< \omega_r \leq 0.866$ p.u. and $T \leq 0.6882$ p.u.: ML operation. (iii) 0.5 p.u. $< \omega_r \leq 0.866$ p.u. and 0.6882 p.u. $< T \leq 0.771$ p.u.: MT operation. (iv) 0.866 p.u $< \omega_r \leq \omega_t$: MT operation. (v) $\omega_r > 0.866$ p.u. and $T \leq 0.5$ p.u.: STP operation.

configuration to avoid a high dc circulating current. The 2L operation does not increase the peak current flowing through the switching devices. However, the 2L operation can increase the rms current flowing through the semiconductor devices. The rms current of the inner device ($S_2$ or $S_3$) increases by $\sqrt{2}$ times. The $S_1$ and $S_5$ or $S_6$ and $S_4$ operate for a full cycle in 2L operation, and the current increment in those devices depends on the modulation index or speed of the operation. In this work, it is assumed that the inverter is capable of operating with the extra rms current flowing through the devices. The motor phase current is always kept limited to the rated value. In the 2L operation, the drive capability and current limits are the same as in the healthy operation.

Considering all the abovementioned modes, the proposed operational zones are shown in Fig. 7. In the case of a switch failure, the inverter is operated in 2L-operation below 0.5 p.u. speed. The operation of the motor is the same as the healthy six-phase operation. Above 0.5 p.u. base speed, the motor is operated with five healthy phases in the $1N$ configuration. The ML and MT operations are considered for torque lesser than 0.688 p.u. and higher than 0.688 p.u., respectively. The maximum possible torque limit is 0.771 p.u. above 0.5 p.u. base speed. The maximum speed limit for ML operation is considered as $\omega_{b,1N}$ (same as $\omega_{b,ml}$). Above $\omega_{b,1N}$, MT operation is used with field weakening till $\omega_t$. $\omega_t$ is the point where achievable torque using MT operation becomes 0.5 p.u.

From (8), (33), the torque at $\omega_t$ in STP operation ($T_{\text{STP,wt}}$) is given as (22)

$$T_{\text{STP,wt}} = \tfrac{3P_l}{2} 0.5 \lambda_m I_m. \tag{22}$$

Similarly, from (8), the torque at $\omega_t$ with MT operation ($T_{\text{MT},wt}$) is given as (23). $i_{d,\omega t}$ and $i_{q,\omega t}$ are the $d$- and $q$-axis current values in MT operation at $\omega_t$, respectively

$$T_{\text{MT},wt} = \tfrac{3P_l}{2} \lambda_m i_{q,\omega t} + (L_d - L_q) i_{q,\omega t} i_{d,\omega t}. \tag{23}$$

As discussed in the MT operation, $|\vec{I_s}| = 0.771 I_m$. Hence, the current equation at $\omega_t$ is given as

$$i_{q,\omega t}^2 + i_{d,\omega t}^2 = (0.771 I_m)^2. \tag{24}$$

At $\omega_t$, the torque from the STP operation is the same as the torque from the MT operation ($T_{\text{STP},wt} = T_{\text{MT},wt}$). Hence, from (22) and (23), the torque equation is given as

$$\tfrac{3P_l}{2} 0.5 \lambda_m I_m = \tfrac{3P_l}{2} \lambda_m i_{q,\omega t} + (L_d - L_q) i_{q,\omega t} i_{d,\omega t}. \tag{25}$$

From (24) and (25), $i_{d,\omega t}$ and $i_{q,\omega t}$ are calculated and given as (26). In (26), for simplification, a variable $k$ is used. $k$ is defined as

$$i_{q,\omega t} = \frac{1 + \sqrt{(1 - 4(1+k)(0.25 + (0.771k)^2))}}{2(1+k)} I_m$$

$$i_{d,\omega t} = -\sqrt{(0.771 I_m)^2 - i_{q,\omega t}^2} \tag{26}$$

$$k = \frac{(L_d - L_q)^2}{\lambda_m^2} I_m^2. \tag{27}$$

From (21), $\omega_t$ is given as

$$\omega_t = \frac{\omega_{b,mt} \lambda_m}{\lambda_m + L_d i_{q,\omega t}}. \tag{28}$$

The motor is operated in STP mode if the speed is above $\omega_t$. The maximum possible torque limit above $\omega_t$ is 0.5 p.u.

## IV. Control Technique for Healthy and Postfault Operation

The healthy and postfault control structure for the SSP-PMSM is shown in Fig. 8. A conventional $dq$ field-oriented control is used to control the speed of the SSP-PMSM in healthy operation. The speed controller generates the torque reference. The $q$-axis current reference is generated from the torque reference using torque constant. In the $1N$ configuration, a zero-axis controller is used to minimize any circulating current between the $RYB$ and $UVW$ phases. The zero sequence current controller is marked in Fig. 8. The control loop is similar to any dual three-phase based PMSM control [18], [29], [30]. In healthy operations, negative sequence currents are not present, and only positive sequence controllers are used. In the postfault operation below 0.5 p.u. speed, the control structure remains the same. However, the PWM technique is modified to operate the inverter in 2L operation.

In the case of MT and ML operation, positive, negative, and zero sequence currents are present [3], [24]. Hence, in MT and ML operations, both positive, negative, and zero sequence current controllers are used. The negative sequence current controller is marked Fig. 8. For conversion between $RYB$ phase components and $dq_{012}$ components, $\theta_r$ is used. The conversion formulas are given in (2) and (3).

For conversion between $RYB$ phase components and negative sequence $dq$ components ($dq_{012}^-$), $\theta_r$ is replaced by $-\theta_r$ in (2) and (3) [3], [24]. The positive and negative sequence current references are generated using the $f(i_{dq012}^{+-})$ block of Fig. 8. The implementation logic of $f(i_{dq012}^{+-})$ block is shown in Fig. 9.

For the reference current generation, the $d$ and $q$-axis current references ($i_q^*$, $i_q^*$) are used. The speed controller generates the torque reference. The $q$-axis current reference is generated from the torque reference using torque constant. The $d$-axis current reference comes from the filed weakening control. The current peak and its phases are calculated from the $dq$-axis

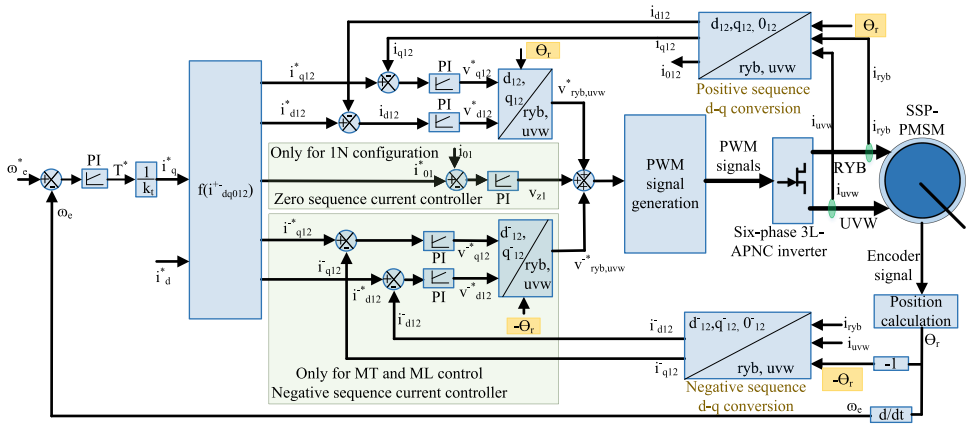


Fig. 8. Speed control diagram of the SSP-PMSM for healthy and postfault operation.

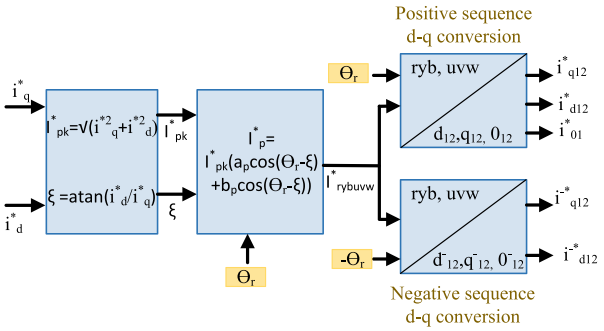


Fig. 9. Block diagram for current reference generation ($f(i^{+-}_{dq012})$).

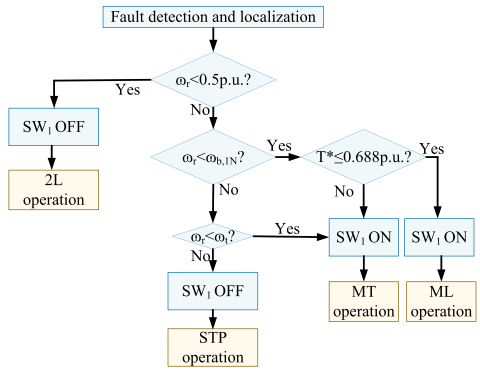


Fig. 10. Flowchart for the postfault operation implementation.

current references using the following equation:

$$I^*_{pk} = \sqrt{i^{*2}_q + i^{*2}_d}$$
$$\xi = a\tan\frac{i^*_d}{i^*_q}. \tag{29}$$

From the current peak and its phases, the phase current references are calculated using the following equation:

$$I^*_p = I^*_{pk}(a_p\cos(\theta_r - \xi) + b_p\sin(\theta_r - \xi)). \tag{30}$$

From the phase current references, the positive-sequence $dq$-axis current references and zero sequence current references are calculated using (2) and (3). For negative sequence $dq$-axis current reference generation $\theta_r$ is replaced by $-\theta_r$ in (2) and (3).

In the postfault operation below 0.5 p.u. speed, the control structure remains the same. However, the PWM technique is modified to operate the inverter in 2L operation. The SSP-PMSM is operated in the $2N$ configuration. When the speed is between $0.5\omega_b$ and $\omega_t$, the motor is operated in MT or ML operation in the $1N$ configuration of SSP-PMSM. Finally, above $\omega_t$ speed, the SSP-PMSM is operated with three phases. The algorithm for implementation of the postfault operation is shown in Fig. 10.

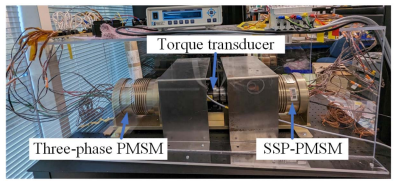


Fig. 11. Experimental motor-generator test setup. An SSP-PMSM is coupled with a three-phase PMSM.

TABLE IV
CALCULATED SPEEDS FOR DIFFERENT CRITICAL POINTS FROM (20) AND (28)

| Parameter | $\omega_b$ | $\omega_{b,\,\mathrm{MT}}$ | $\omega_t$ | $\omega_{t,\,\mathrm{STP}}$ |
|---|---|---|---|---|
| Value | 6000 r/min (1p.u.) | 5190 r/min (0.866p.u.) | 5370 r/min (0.895p.u.) | 6000 r/min (1p.u.) |

## V. EXPERIMENTAL RESULTS

The postfault operational technique is validated in a GaN-based 3L-ANPC inverter-driven SSP-PMSM. Fig. 11 shows the picture of the SSP-PMSM. The motor parameters are provided in Table III. The motor has a base speed of 6000 r/min ($\omega_b = 2513$ rad/s corresponds to 400 Hz fundamental frequency). Different calculated critical speeds are given in Table IV. The SSP-PMSM is coupled with a three-phase PMSM, which is used

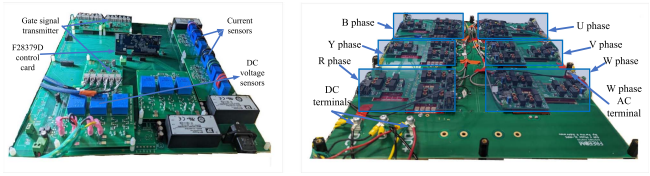


(a) (b)

Fig. 12. Experimental test setup. (a) TI-DSP TMS320F28379D-based DSP board with voltage and current sensors. (b) 650 V GaN device-based six-phase 3L-ANPC inverter.

TABLE V
CONTROL IMPLEMENTATION PARAMETERS

| Parameter | Switching frequency | Sampling frequency | Controller execution time |
|---|---|---|---|
| Value | 50 kHz | 50 kHz | $14\mu s$ in healthy operation. $17\mu s$ in postfault operation. |

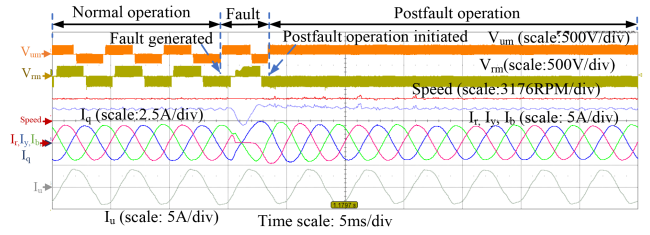


Fig. 13. Pole voltage and current waveforms for $S_1$ open-switch fault in the $R$ phase at 3000 r/min (0.5 p.u.) with 0.85 p.u. loading. In the postfault operation, the inverter generates 2L pole voltage. The current remains the same as the normal operation.

for loading the SSP-PMSM. A three-phase resistive load is connected to the three-phase PMSM to generate a speed-dependent loading of the SSP-PMSM. Operations at different loads are achieved by changing the load resistance of the three-phase PMSM. As the loading is done using a three-phase resistive load at any speed with a constant resistance value, the output shaft torque remains constant, irrespective of the operational mode. The SSP-PMSM is controlled using a GaN-based 3L-ANPC inverter. GaN systems 650 V/60 A bottom cool GaN devices GS66516B are used for designing the 3L-ANPC inverter. The inverter is supplied from a 400 V dc source and operated at a 50 kHz switching frequency. The control technique is implemented in industry-grade TI's DSP TMS320F28379D. The DSP board with sensors is shown in Fig. 12(a). The six-phase inverter is shown in Fig. 12(b). The current controllers are implemented in a 50 kHz interrupt service routine (ISR). The speed controller is implemented in a 1 kHz ISR. The DSP has an internal clock frequency of 200 MHz. The execution time for the control loop with the proposed algorithm is $\approx 14\,\mu$s in a healthy operation. Due to the negative sequence current controllers, the execution time increases in the postfault operation. In the postfault operations, the execution time is $\approx 17\mu$s. The controller implementation details are shown in Table V.

Fig. 13 shows experimental results at 3000 r/min (0.5 p.u. speed) with 0.85 p.u. load (3 A rms current). The SSP-PMSM is operated in the $2N$ configuration. In healthy operation, both

TABLE VI
MECHANICAL PARAMETER OF THE MOTOR GENERATOR SET

| Parameter | B (m·N–ms/rad) | J (m·N–ms$^2$/rad) | Mechanical time constant (J/B) (ms) |
|---|---|---|---|
| Value | 0.138 | 16.48 | 119 |

$R$ and $U$ phases have 3L switching voltages. Both pole voltage switches between $P$, $O$, and $N$. An OCF is generated by turning OFF $S_1$ device of the $R$ phase (see Fig. 1). The effect of the fault can be observed only when the switching happens between $P$ and 0 or the positive half of the fundamental cycle. After the OCF generation, the positive half of the $R$ phase current gets clamped to zero. In the fault duration, the $R$ phase pole voltage switches between $P$ ($V_{dc}/2$) and 0. In this work, the fault is generated by removing the gate pulse of the $R$ phase $S_1$ device. The other device gate pulses remain the same. The faulty device remains connected, and the current flow in the negative direction (through the diode or third quadrant current) is possible. Due to the ripple negative current through the device (diode) of $S_1$ of the $R$ phase, voltage still shows a positive value ($V_{dc}/2$) in the fault region before switching to 2L operation.

The motor mechanical parameters are given in Table VI. The mechanical time constant of the motor is 119 ms. The transient time in the $q$-axis current in Fig. 13 is 2.5 ms. Due to the short transient time and high mechanical time constant, the change in the motor speed is negligibly small and not observable in Fig. 13.

A delay of 5 ms (one fundamental cycle) is provided between the fault generation and the initiation of the postfault control. As OCF is considered in the $S_1$ device of the $R$ phase, till $0.5\omega_b$ the $RYB$ phases should switch between 0 and $N$, and the $UVW$ phases should switch between $P$ and 0. In the postfault operation, the $R$ phase pole voltage switches between 0 and $N$, and the $U$ phase pole voltage switches between $P$ and 0. In the postfault operation, the $q$-axis and the phase currents remain the same as in the healthy operation. The faulty $R$ phase also has the same current as the healthy operation. The result ensures the generation of the same current below 0.5 p.u. speed. The $q$-axis current ($I_q$) represents the torque component. The $q$-axis current in postfault operation is the same as in healthy operation. The $q$-axis current value is 4.24 A (3A $\times \sqrt{2}$) during both healthy and postfault operations. The measured shaft torque is 3.64 N · m. The shaft torque and the $q$-axis current remain the same in both healthy and postfault operations.

Fig. 14 shows the postfault operation when the speed changes from 2250 r/min (0.375 p.u.) to 5400 r/min (0.9 p.u.). The fault is considered in the $S_4$ device of the $R$ phase. Till the 3000 r/min (0.5 p.u.) speed, the inverter operates in the 2L operational mode in the $2N$ configuration of the SSP-PMSM. The $U$ phase voltage switches between 0 and $N$ ($-V_{dc}/2$). The zoomed waveform at 2250 r/min is shown in Fig. 15(a). Till 3000 r/min, the currents are observed in all six phases. The SSP-PMSM is operated in the $2N$ configuration. Hence, no current flows between $N1$ and $N2$. In Fig. 15(a), the rms of the six-phase currents is 937 mA ($\pm 2\%$) (0.27 p.u.). As balanced six-phase current flows, the $I_q$ current value is also 1.32A ($0.937A \times \sqrt{2}$). The measured shaft torque is 1.59 N · m.

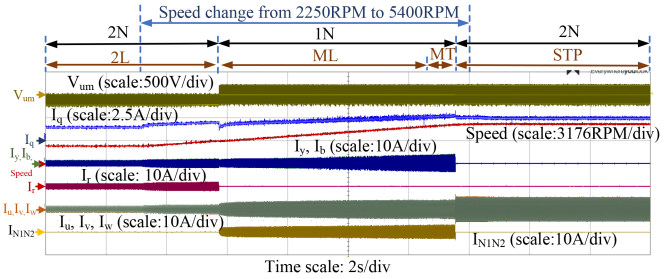


Fig. 14. Postfault operation for $S_4$ of $R$ phase $OCF$. The speed is changed from 2250 r/min (0.375 p.u.) to 5400 r/min (0.9 p.u.). The inverter is operated in the 2L operation till 3000 r/min (0.5 p.u.). Between 3000 r/min (0.5 p.u.) and 5190 r/min (0.866 p.u.) The drive is operated in the ML operation. Between 5190 r/min (0.866 p.u.) and 5370 r/min ($\omega_t$) the drive is operated in the MT operation. Above 5370 r/min ($\omega_t$), the inverter is operated in STP mode. The load is selected such that at STP mode, the load of the SSP-PMSM reaches 0.5 p.u. or rated current in healthy three phases.

Over 3000 r/min (0.5 p.u.) speed, the SSP-PMSM is operated in the $1N$ configuration with five healthy phases. Consequently, the $R$ phase current becomes zero. The motor is operated in the ML operational mode till 5190 r/min (0.866 p.u.) in the $1N$ configuration. Between 5190 r/min (0.866 p.u.) and 5370 r/min ($\omega_t$), the motor is operated in the MT operational mode. During ML and MT operational modes, fundamental frequency current flows between $N1$ and $N2$. The ML operation at 4500 r/min (0.75 p.u.) is shown in Fig. 15(b). In Fig. 15(b), the maximum rms current of 2.17 A (0.613 p.u.) flows in the $U$ phase. The $q$-axis ($I_q$) current value is 2.11 A (0.422 p.u.) ($2.11 = 2.17 \times \sqrt{2} \times 0.688$). The measured shaft torque is 2.94 N $\cdot$ m.

The MT operation at 5250 r/min (0.875 p.u.) is shown in Fig. 15(c). The measured shaft torque is 3.31 N $\cdot$ m. Above 5370 r/min ($\omega_t$), the motor operates in STP operational mode. Consequently, the $R$, $Y$, and $B$ phase current becomes zero. The STP operational mode results at 5400 r/min (0.9 p.u.) speed is shown in Fig. 15(d). In Fig. 15(d), the rms current of $UVW$ phases is 3.54 A (1 p.u.). The $q$-axis current ($I_q$) is 2.5 A ($2.5 = 3.54 \times \sqrt{2} \times 0.5$). In Fig. 14, the motor speed is kept limited to 5400 r/min (0.9 p.u.), as at 5400 r/min speed in the considered loading condition, the $UVW$ phase current becomes 1 p.u. (3.54 A rms). The measured shaft torque is 3.37 N $\cdot$ m. The operation in the entire operating range is shown in Fig. 16 in no-load operation. In Fig. 16, the speed is changed from 1500 r/min (0.25 p.u.) to 6150 r/min (1.025 p.u.). The inverter operates in 2L mode till 3000 r/min (0.5 p.u.). The motor operates in ML mode till 5190 r/min (0.866 p.u.) and MT mode till 5370 r/min ($\omega_t$). Above 5370 r/min ($\omega_t$) speed, the converter operates in the STP operational mode.

Fig. 17 shows experimental results at 4500 r/min (0.75 p.u.) with 0.68 p.u. load. Fig. 17(a) shows experimental results in healthy operating conditions. The SSP-PMSM is controlled in the $2N$ configuration. Consequently, no current flows between $N1$ and $N2$. The same rms current ($2.41A \pm 1.5\%$) (0.68 p.u.) flows in all the phases six phases. The $q$-axis current is 3.4 A(0.68 p.u.). Fig. 17(b) shows the experimental result for an OCF in the $R$ phase in the ML operation. In ML operation, different rms current flows in all five healthy phases.

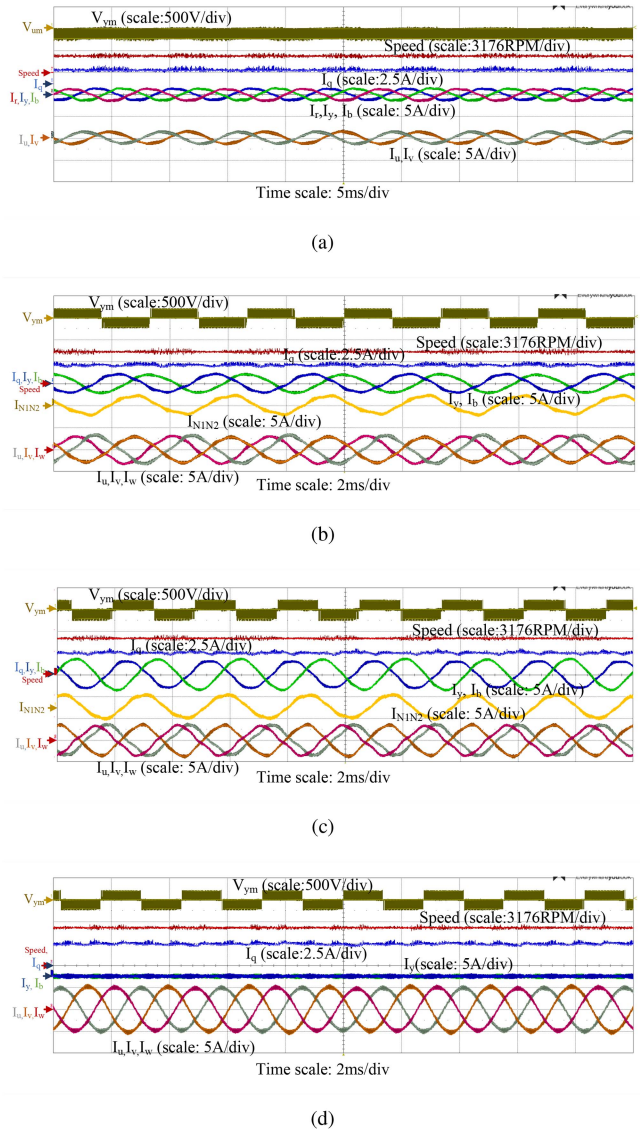


Fig. 15. Voltage and current waveform at different speeds of Fig. 14. (a) 2L operation at 2250 r/min (0.375 p.u.) In 2L operation, the current in the faulty $R$ phase flows like normal operation. (b) ML operation at 4500 r/min (0.75 p.u.). The faulty $R$ phase current is zero, and the fundamental frequency current flows between $N1$ and $N2$. (c) MT operation at 5250 r/min (0.875 p.u.). The faulty $R$ phase current is zero, and the fundamental frequency current flows between $N1$ and $N2$. (d) STP operation at 5400 r/min (0.9 p.u.). Rated current flows in the $UVW$ phases. No current flows in $RYB$ phases.

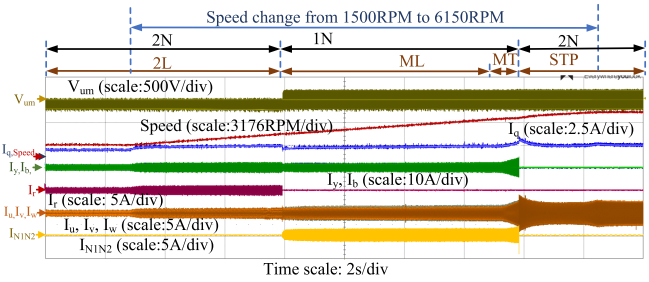


Fig. 16. Postfault operation for $S_4$ of $R$ phase OCF in no load. The speed is changed from 2250 r/min (0.375 p.u.) to 6150 r/min (1.025 p.u.).

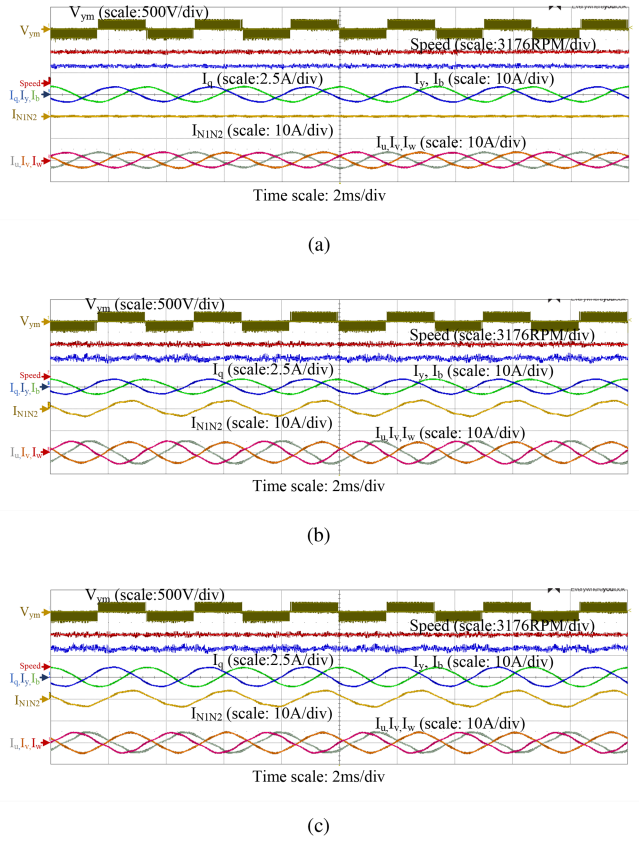


Fig. 17. Voltage and current waveform of the SSP-PMSM at 4500 r/min (0.75 p.u) with 0.68 p.u. load in different operations. (a) Normal operation. (b) ML operation. (c) MT operation.

The maximum current flows in the $U$ phase. The rms current in the $U$ phase is 3.52 A (0.994 p.u.) ($3.52 \approx 2.41/0.688$). The minimum current of 2.41 A (0.68 p.u.) flows in the $Y$ and $B$ phases. The $q$-axis current is the same as that of a healthy operation (3.4 A). A fundamental frequency current of 2.41 A rms (0.68 p.u.) flows between $N1$ and $N2$. Fig. 17(c) shows the experimental result in MT operation at the same operating points. In MT operation, all five healthy phases should have the same current. All five phases have $3.12A \pm 1.3\%$ (0.881 p.u.) rms current ($3.12 \approx 2.41/0.771$). A fundamental frequency current of 2.55 A rms (0.72 p.u.) flows between $N1$ and $N2$. As the loading condition is the same, the $q$-axis current in normal, MT, and ML operations are the same (3.4 A). The low-frequency ripple in the $q$-axis current in ML and MT operation is the same as in healthy operation. The measured shaft torque for all three operational modes in Fig. 17 is 2.94 N · m. The $q$-axis current in all three results is 3.41 A. The output torque and $q$-axis current are constant at constant speed.

The efficiency variation of the system (inverter+motor) for an OCF in the $R$ phase at different speeds in MT and ML operations is shown in Fig. 18. The test condition is the same as in Fig. 17. At 4500 r/min (0.75 p.u. speed), the ML operation has 0.4% higher efficiency than the MT operation.

Table VII shows the comparison with the existing literature. Fig. 13 shows the experimental result in the 2L operation. The

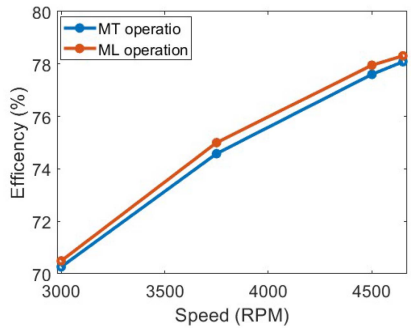


Fig. 18. System efficiency variation with speed in MT and ML operation. At 4500 r/min (0.75 p.u. speed), the ML operation has 0.4% higher efficiency than the MT operation.

TABLE VII
COMPARISON OF POSTFAULT OPERATIONS OF SIX-PHASE MOTOR DRIVES

| Reference | Six-phase operation (Full torque) below 0.5p.u. speed | Full speed operation | Both $1N$ and $2N$ operation | Additional hardware requirement |
|---|---|---|---|---|
| [19] | No | Yes | No | No |
| [20] | No | Yes | No | No |
| [21] | No | Yes | Yes | No |
| [22] | Yes | No | Yes | Yes |
| **This article** | **Yes** | **Yes** | **Yes** | **No** |

The bold text highlights the applicability of this article with that of the literature.

results show even after a device fault, the motor has current in all six phases and can generate the same torque, which is not possible with the methods of [19], [20], [21]. The method of [22] can generate all six-phase currents but needs additional hardware to connect the faulty phase to the midpoint of the dc bus. The proposed method of this article does not need additional hardware to connect the faulty phase pole to the midpoint of the dc bus.

The proposed method allows postfault operation above base speed by operating at STP mode, which is not possible using the method of [22]. The result is shown in Fig. 16. The maximum speed operation is possible by operating the motor in the $2N$ configuration [19], [20], [21]. However, operation at $2N$ configuration limits the torque to 0.5 p.u. for SSP-PMSM and 0.577 for ASP-PMSM. The torque can be increased by operating the motor in the $1N$ configuration. Operation in both $1N$ and $2N$ configurations is not discussed in [19] and [20].

Both $1N$ and $2N$ configuration operations are considered in this work. The proposed method maximized the torque by operating in the $1N$ configuration below critical speed ($\omega_t$). The proposed method also maximized the speed by operating in the STP mode above critical speed ($\omega_t$). The proposed method also enables all six-phase operations (full torque) below 0.5 p.u. speed that does not need any additional hardware.

## VI. CONCLUSION

An open-switch postfault operational technique with the enhanced torque–speed region for 3L-ANPC inverter-driven SSP-PMSM is presented in this article. In case of an open-switch

fault of SSP-PMSM, the faulty phase is commonly disconnected, and the motor is operated with the remaining five healthy phases. Operating with healthy five phases limits the maximum possible output torque to 0.5 p.u. in the $2N$ configuration. The output torque can be increased to 0.771 p.u. by operating the SSP-PMSM in the $1N$ configuration. However, the $1N$ configuration limits the maximum possible speed below 1 p.u. In this article, hardware and software modifications are used to enhance the torque–speed operating region during postfault operation. Below 0.5 p.u. speed, modification in the PWM technique is used to achieve 1 p.u. torque. Above 0.5 p.u. speed, MT, and ML operations are used in the $1N$ configuration of the SSP-PMSM to maximize the torque output till a critical speed ($\omega_t$). The maximum possible torque limit from 0.5 to 0.866 p.u. speed is 0.771 p.u. Finally, above the critical speed, STP operation is used to maximize the speed limit in postfault operation. The proposed postfault operational technique has the following advantages.

1) In the postfault operation, the proposed technique enables 1 p.u. torque generation below 0.5 p.u. speed. Consequently, compared to the operation with healthy five phases, the torque output limit increases by 29.7%.
2) Above 0.5 p.u. speed, the proposed technique maximizes the torque output limit to 0.771 p.u. by operating the SSP-PMSM in the $1N$ configuration.
3) The proposed technique maximizes the speed output limit by operating the inverter in the STP mode above critical speed ($\omega_t$). The STP operation enables operation at 1 p.u. speed without field weakening (increased by 15.47% from 0.866 to 1 p.u.).

The proposed postfault operational technique enhances both torque and speed limit without the need for any additional hardware to connect the faulty phase pole to the midpoint of the dc bus.

## APPENDIX

### A. STP Operation

In the case of the STP operation, the three-phase set, which consists of the faulty phase, is turned-OFF. In the case of a fault in the $R$ phase, $RYB$ phases are turned-OFF. Hence, the $a_p$ and $b_p$ for the $RYB$ phases become zero. To generate 1 p.u. torque, $a_p$ and $b_p$ of $UVW$ phases should follow (10). $a_p$ and $b_p$ values for $UVW$ phases are calculated by solving (10) and (11) and given as (31). MATLAB is used to determine the solutions to the equations

$$a_u=1 \quad b_u=\sqrt{3} \quad a_v=-2 \quad b_v=0 \quad a_w=1 \quad b_w=-\sqrt{3}. \tag{31}$$

Equation (31) needs to be followed to generate 1 p.u. torque in the STP operation. However, in (31) $k_p=\sqrt{a_p^2+b_p^2}$ is higher than 1. $k_p$ greater than one represents, the current value of the $p$ phase is higher than the rated value. To keep phase current values limited to 1 p.u. for all the phases, $a_p$ and $b_p$ values of all six phases are divided by max $\left[\sqrt{a_p^2+b_p^2}\right]$. Hence, the modified values of $a_p$ and $b_p$ for $UVW$ phases are given as (32). The values of (32) should be used for STP operation

$$a_{u,\text{STP}}=\frac{1}{2} \quad b_{u,\text{STP}}=\frac{\sqrt{3}}{2} \quad a_{v,\text{STP}}=-\frac{1}{2}$$
$$b_{v,\text{STP}}=0 \quad a_{w,\text{STP}}=\frac{1}{2} \quad b_{w,\text{STP}}=-\frac{\sqrt{3}}{2}. \tag{32}$$

Replacing the values of (32) in (4), the calculated current vector is $|\vec{I}_s|=0.5I_m$. From (8), the maximum possible torque in STP operation is given as (33). Hence, the maximum possible torque capability in the STP operation ($T_{\text{stp,max}}$) is $\frac{T_{\text{stp,max}}}{T}=0.5$ p.u. when the phase currents are limited to 1 p.u.

$$T_{\text{stp,max}}=K_t|\vec{I}_s|=0.5K_tI_m. \tag{33}$$

### B. MT Operation

In MT operation $a_p$ and $b_p$ are given as (13) for the $R$ phase failure. For 1 p.u. torque generation, the $a_p$ and $b_p$ values are calculated using (10), (11), and (13) for the $1N$ configuration and are given as (34). MATLAB is used to determine the solutions to the equations

$$a_y=-0.527 \quad b_y=1.185 \quad a_b=-0.527 \quad b_b=-1.185$$
$$a_u=1.176 \quad b_u=0.547 \quad a_v=-1.297 \quad b_v=0$$
$$a_w=1.176 \quad b_w=-0.547. \tag{34}$$

However, the $k_p$ value in (34) is 1.279. $k_p=1.279$ represents the required phase current values are 27.9% higher than the rated value for 1p.u. torque generation. Similar to the STP operation, to keep the phase current values limited to 1 p.u. for all the phases, the $a_p$ and $b_p$ values are divided by max$[\sqrt{a_p^2+b_p^2}]$. The modified $a_p$ and $b_p$ are given as (35). The values of (35) should be used for MT operation

$$a_{y,\text{MT}}=-0.407 \quad b_{y,\text{MT}}=0.914 \quad a_{b,\text{MT}}=-0.407$$
$$b_{b,\text{MT}}=-0.917 \quad a_{u,\text{MT}}=0.907 \quad b_{u,\text{MT}}=0.422$$
$$a_{v,\text{MT}}=-1 \quad b_{v,\text{MT}}=0 \quad a_{w,\text{MT}}=0.914$$
$$b_{w,\text{MT}}=-0.407. \tag{35}$$

Replacing the values of (35) in (4), the calculated current vector is $|\vec{I}_s|=0.771I_m$. The maximum possible torque capability in MT operation is $\frac{T_{\text{MT,max}}}{T}=0.771$ p.u. when the phase currents are limited to 1 p.u.

Similarly, $a_p$ and $b_p$ values are calculated for the $2N$ configuration in MT operation. The torque limit is calculated as 0.5 p.u. As the torque limit is less than the $1N$ configuration, the MT operation in the $2N$ configuration is not further considered in this work.

### C. ML Operation

For ML operation, stator copper loss is minimized for a given torque. The MATLAB optimization toolbox is used for $a_p$ and $b_p$ determination, where the optimization target is given to minimize $J$ [copper loss coefficient defined by (14)]. Equations (10) and (11) are given as constraints. The calculated $a_p$ and $b_p$

values are given as (36) for 1 p.u. torque generation

$$\begin{aligned} &a_y = -0.5 \quad b_y = 0.866 \quad a_b = -0.5 \quad b_b = -0.866 \\ &a_u = 1.167 \quad b_u = 0.866 \quad a_v = -1.333 \quad b_v = 0 \\ &a_w = 1.167 \quad b_w = -0.866. \end{aligned} \tag{36}$$

However, the $k_p$ value in (34) is 1.453 for the $U$ phase. $k_p = 1.453$ represents that the required phase current value is 45.3% higher than the rated values of 1 p.u. torque generation. Similar to the STP and MT operations, to keep the current values below 1 p.u. for all the phases, the $a_p$ and $b_p$ values are divided by $\max\left[\sqrt{a_p^2 + b_p^2}\right]$. The modified $a_p$ and $b_p$ are given as (37). The values of (37) should be used for ML operation

$$\begin{aligned} &a_{y,\mathrm{ML}} = -0.344 \quad b_{y,\mathrm{ML}} = 0.596 \quad a_{b,\mathrm{ML}} = -0.344 \\ &b_{b,\mathrm{ML}} = -0.596 \quad a_{u,\mathrm{ML}} = 0.803 \quad b_{u,\mathrm{ML}} = 0.596 \\ &a_{v,\mathrm{ML}} = -0.918 \quad b_{v,\mathrm{ML}} = 0 \quad a_{w,\mathrm{ML}} = 0.803 \\ &b_{w,\mathrm{ML}} = -0.596. \end{aligned} \tag{37}$$

Replacing the values of (37) in (4), the calculated maximum current vector is $|\vec{I_s}| = 0.688 I_m$. The maximum possible torque capability in ML operation is $\frac{T_{\mathrm{ML,max}}}{T} = 0.688$ p.u. when the phase currents are limited to 1 p.u.

Similarly, $a_p$ and $b_p$ values are calculated for the $2N$ configuration with ML operation. The torque limit is calculated as 0.5 p.u. As the torque limit is less than the $1N$ configuration, the ML operation in the $2N$ configuration is not considered further.

## REFERENCES


[1] A. Salem and M. Nariman, "A review on multiphase drives for automotive traction applications," *IEEE Trans. Transport. Electrific.*, vol. 5, no. 4, pp. 1329–1348, Dec. 2019.

[2] E. Levi, "Multiphase electric machines for variable-speed applications," *IEEE Trans. Ind. Electron.*, vol. 55, no. 5, pp. 1893–1909, May 2008.

[3] W. N. W. A. Munim, M. J. Duran, H. S. Che, M. Bermúdez, I. González-Prieto, and N. A. Rahim, "A unified analysis of the fault tolerance capability in six-phase induction motor drives," *IEEE Trans. Power Electron.*, vol. 32, no. 10, pp. 7824–7836, Oct. 2017.

[4] P. P. Das, S. Satpathy, S. Bhattacharya, and V. Veliadis, "Design considerations of multi-phase multilevel inverters for high-power density traction drive applications," in *Proc. IEEE Transp. Electrific. Conf. Expo.*, 2022, pp. 23–30.

[5] W. Taha, P. Azer, A. Poorfakhraei, S. Dhale, and A. Emadi, "Comprehensive analysis and evaluation of DC-link voltage and current ripples in symmetric and asymmetric two-level six-phase voltage source inverters," *IEEE Trans. Power Electron.*, vol. 38, no. 2, pp. 2215–2229, Feb. 2023.

[6] A. González-Prieto, I. González-Prieto, A. G. Yepes, M. J. Duran, and J. Doval-Gandoy, "On the advantages of symmetrical over asymmetrical multiphase AC drives with even phase number using direct controllers," *IEEE Trans. Ind. Electron.*, vol. 69, no. 8, pp. 7639–7650, Aug. 2022.

[7] S. Satpathy, S. Bhattacharya, and V. Veliadis, "Comprehensive loss analysis of two-level and three-level inverter for electric vehicle using drive cycle models," in *Proc. 46th Annu. Conf. IEEE Ind. Electron. Soc.*, 2020, pp. 2017–2024.

[8] A. Kersten et al., "Fault detection and localization for limp home functionality of three-level NPC inverters with connected neutral point for electric vehicles," *IEEE Trans. Transport. Electrific.*, vol. 5, no. 2, pp. 416–432, Jun. 2019.

[9] A. K. Morya et al., "Wide bandgap devices in AC electric drives: Opportunities and challenges," *IEEE Trans. Transport. Electrific.*, vol. 5, no. 1, pp. 3–20, Mar. 2019.

[10] X. Liu, F. Yu, J. Mao, and H. Yang, "Pre- and post-fault operations of six-phase electric-drive-reconstructed onboard charger for electric vehicles," *IEEE Trans. Transport. Electrific.*, vol. 8, no. 2, pp. 1981–1993, Jun. 2022.

[11] J. W. Bennett, G. J. Atkinson, B. C. Mecrow, and D. J. Atkinson, "Fault-tolerant design considerations and control strategies for aerospace drives," *IEEE Trans. Ind. Electron.*, vol. 59, no. 5, pp. 2049–2058, May 2012.

[12] J. A. Swanke and T. M. Jahns, "Reliability analysis of a fault-tolerant integrated modular motor drive for an urban air mobility aircraft using Markov chains," *IEEE Trans. Transport. Electrific.*, vol. 8, no. 4, pp. 4523–4533, Dec. 2022.

[13] Z. Zhou and S. Yao, "Deadbeat direct current control using dynamic time programming for six-phase PMSM drives with open-phase faults," *IEEE Trans. Ind. Electron.*, vol. 71, no. 9, pp. 10064–10074, Sep. 2024.

[14] G. Feng, C. Lai, W. Li, J. Tjong, and N. C. Kar, "Open-phase fault modeling and optimized fault-tolerant control of dual three-phase permanent magnet synchronous machines," *IEEE Trans. Power Electron.*, vol. 34, no. 11, pp. 11116–11127, Nov. 2019.

[15] S. Jin, W. Zhao, J. Ji, and D. Xu, "Deadbeat fault-tolerant control scheme for dual three-phase PMSG with high-resistance connection fault," *IEEE Trans. Power Electron.*, vol. 38, no. 3, pp. 4015–4026, Mar. 2023.

[16] H. Mesai-Ahmed, I. Jlassi, A. J. M. Cardoso, and A. Bentaallah, "Multiple open-circuit faults diagnosis in six-phase induction motor drives using stator current analysis," *IEEE Trans. Power Electron.*, vol. 37, no. 6, pp. 7275–7285, Jun. 2022.

[17] J. Sun, C. Li, Z. Zheng, K. Wang, and Y. Li, "A generalized, fast and robust open-circuit fault diagnosis technique for star-connected symmetrical multiphase drives," *IEEE Trans. Energy Convers.*, vol. 37, no. 3, pp. 1921–1933, Sep. 2022.

[18] P. P. Das, S. Satpathy, and S. Bhattacharya, "An online open-circuit fault diagnosis technique for three-level inverter-fed six-phase PMSM drives," *IEEE Trans. Power Electron.*, vol. 39, no. 11, pp. 14974–14987, Nov. 2024.

[19] Q. Geng, Z. Li, H. Wang, G. Zhang, and Z. Zhou, "Natural fault-tolerant control with minimum copper loss in full torque operation range for dual three-phase PMSM under open-circuit fault," *IEEE Trans. Power Electron.*, vol. 39, no. 1, pp. 1279–1291, Jan. 2024.

[20] Y. Hu, Y. Feng, and X. Li, "Fault-tolerant hybrid current control of dual three-phase PMSM with one phase open," *IEEE Trans. Emerg. Sel. Topics Power Electron.*, vol. 10, no. 3, pp. 3418–3426, Jun. 2022.

[21] H. M. Eldeeb, A. S. Abdel-Khalik, and C. M. Hackl, "Postfault full torque–speed exploitation of dual three-phase IPMSM drives," *IEEE Trans. Ind. Electron.*, vol. 66, no. 9, pp. 6746–6756, Sep. 2019.

[22] A. G. Yepes, J. Doval-Gandoy, and H. A. Toliyat,, "Strategy with smooth transitions and improved torque–speed region and stator copper loss for two-level asymmetrical six-phase induction motor drives under switch faults," *IEEE Trans. Power Electron.*, vol. 36, no. 2, pp. 1954–1969, Feb. 2021.

[23] X. Wang, Z. Wang, Z. Xu, J. He, and W. Zhao, "Diagnosis and tolerance of common electrical faults in t-type three-level inverters fed dual three-phase PMSM drives," *IEEE Trans. Power Electron.*, vol. 35, no. 2, pp. 1753–1769, Feb. 2020.

[24] H. S. Che, M. J. Duran, E. Levi, M. Jones, W.-P. Hew, and N. A. Rahim, "Postfault operation of an asymmetrical six-phase induction machine with single and two isolated neutral points," *IEEE Trans. Power Electron.*, vol. 29, no. 10, pp. 5406–5416, Oct. 2014.

[25] E. Levi, D. Dujic, M. Jones, and G. Grandi, "Analytical determination of DC-bus utilization limits in multiphase VSI supplied AC drives," *IEEE Trans. Energy Convers.*, vol. 23, no. 2, pp. 433–443, Jun. 2008.

[26] X. Wang et al., "Fault-tolerant control of common electrical faults in dual three-phase PMSM drives fed by t-type three-level inverters," *IEEE Trans. Ind. Appl.*, vol. 57, no. 1, pp. 481–491, Jan./Feb. 2021.

[27] J.-R. Fu and T. A. Lipo, "Disturbance-free operation of a multiphase current-regulated motor drive with an opened phase," *IEEE Trans. Ind. Appl.*, vol. 30, no. 5, pp. 1267–1274, Sep./Oct. 1994.

[28] P. P. Das, S. Satpathy, and S. Bhattacharya, "A six-phase space vector PWM technique for wide-bandgap device-based three-level inverters," *IEEE Trans. Transport. Electrific.*, vol. 10, no. 3, pp. 5819–5830, Sep. 2024.

[29] P. Pillay and R. Krishnan, "Modeling, simulation, and analysis of permanent-magnet motor drives. I. the permanent-magnet synchronous motor drive," *IEEE Trans. Ind. Appl.*, vol. 25, no. 2, pp. 265–273, Mar./Apr. 1989.

[30] R. Bojoi, M. Lazzari, F. Profumo, and A. Tenconi, "Digital field-oriented control for dual three-phase induction motor drives," *IEEE Trans. Ind. Appl.*, vol. 39, no. 3, pp. 752–760, May/Jun. 2003.

**Partha Pratim Das** (Member, IEEE) received the B.Tech. degree from the West Bengal University of Technology, Kolkata, India, in 2012, the M.S. degree from the Indian Institute of Technology Kharagpur, Kharagpur, India, in 2016, and the Ph.D. degree from North Carolina State University, Raleigh, NC, USA, in 2024, all in electrical engineering.

He was a Senior Engineer with Delta Power Solution, Bangalore, India, from 2016 to 2019. He is currently a Postdoctoral Research Scholar with the NSF FREEDM Systems Center, North Carolina State University, Raleigh, NC, USA. His research interests include the design and control of reliable and fault-tolerant power electronics converters and motor drives using silicon and wideband gap devices for transportation and renewable energy applications.

**Subhransu Satpathy** (Member, IEEE) received the B.Tech degree from the National Institute of Technology, Rourkela, India, in 2013, the M.S. degree from the Indian Institute of Technology Madras, Chennai, India, in 2018, and the Ph.D. degree from North Carolina State University, Raleigh, NC, USA, in 2024, all in electrical engineering.

From 2017 to 2019, he was with Eaton India Innovation Center, Pune, India. He is currently an Application Engineer with the GaN team, Texas Instruments Inc., Dallas, TX, USA. His research interests include GaN-based power converter design, dc–dc/dc–ac power conversion topologies, PWM techniques, and high-speed electric drives.

**Subhashish Bhattacharya** (Fellow, IEEE) received the B.E. degree from the Indian Institute of Technology Roorkee, Roorkee, India, in 1986, the M.E. degree from the Indian Institute of Science, Bengaluru, India, in 1988, and the Ph.D. degree from the University of Wisconsin-Madison, Madison, WI, USA, in 2003, all in electrical engineering.

He was with the FACTS and the Power Quality Group, Westinghouse, which later became part of Siemens Power, from 1998 to 2005. In 2005, he joined the Department of ECE, NCSU where he is currently a Duke Energy Distinguished Professor and a Founding Faculty Member of NSF ERC FREEDM Systems Center, Advanced Transportation Energy Center (ATEC), and the U.S. DOE initiative on WBG-based Manufacturing Innovation Institute-Power America, NCSU. His research is funded by several industries, including NSF, DoE, ARPA-E, U.S. Navy, ONR, and NASA. He has more than 800 publications, H-index of 77, and 24,800+ citations. His research interests include solid-state transformers, integration of renewable energy resources, MV power converters enabled by HV SiC devices, FACTS, utility applications of power electronics and power quality issues, dc microgrids, high-frequency magnetics, active filters, and application of new power semiconductor devices, such as SiC and GaN for converter topologies.